International Journal of Nanomedicine

Dovepress
open access to scientific and medical research

Open Access Full Text Article

ORIGINAL RESEARCH

The Effects of a Novel Curcumin Derivative Loaded Long-Circulating Solid Lipid Nanoparticle on the MHCC-97H Liver Cancer Cells and Pharmacokinetic Behavior

Yumeng Wei[1–3,*], Ke Li[1–3,*], Wenmei Zhao[1–3,*], Yingmeng He[2,4], Hongping Shen[2,5], Jiyuan Yuan[2,5], Chao Pi[1–3], Xiaomei Zhang[6], Mingtang Zeng[1–3], Shaozhi Fu[7], Xinjie Song[8,9], Robert J Lee[10], Ling Zhao[2,3]

[1]Key Laboratory of Medical Electrophysiology, Ministry of Education, School of Pharmacy of Southwest Medical University, Luzhou, Sichuan, 646000, People's Republic of China; [2]Luzhou Key Laboratory of Traditional Chinese Medicine for Chronic Diseases Jointly Built by Sichuan and Chongqing, the Affiliated Traditional Chinese Medicine Hospital of Southwest Medical University, Luzhou, Sichuan, 646000, People's Republic of China; [3]Central Nervous System Drug Key Laboratory of Sichuan Province, Southwest Medical University, Luzhou, Sichuan, 646000, People's Republic of China; [4]Department of Pharmacy, the Affiliated Traditional Chinese Medicine Hospital of Southwest Medical University, Luzhou, Sichuan, 646000, People's Republic of China; [5]Clinical Trial Center, the Affiliated Traditional Chinese Medicine Hospital of Southwest Medical University, Luzhou, Sichuan, 646000, People's Republic of China; [6]Luzhou Key Laboratory of Traditional Chinese Medicine for Chronic Diseases Jointly Built by Sichuan and Chongqing, Institute of Medicinal Chemistry of Chinese Medicine, Chongqing Academy of Chinese Materia Medica, Chongqing, 400065, People's Republic of China; [7]Department of Oncology, the Affiliated Hospital of Southwest Medical University, Luzhou, Sichuan, 646000, People's Republic of China; [8]School of Biological and Chemical Engineering, Zhejiang University of Science and Technology, Hangzhou, Zhejiang, 310023, People's Republic of China; [9]Department of Food Science and Technology, Yeungnam University, Gyeongsan-si, Gyeongsangbuk-do, 38541, Republic of Korea; [10]Division of Pharmaceutics and Pharmacology, College of Pharmacy, the Ohio State University, Columbus, OH, 43210, USA

*These authors contributed equally to this work

Correspondence: Robert J Lee, The Ohio State University, 500 W 12th Ave, Columbus, OH, 43210, USA, Tel +1-614-292-4172, Fax +1-614-292-4172, Email lee.1339@osu.edu; Ling Zhao, Luzhou Key Laboratory of Traditional Chinese Medicine for Chronic Diseases Jointly Built by Sichuan and Chongqing, the Affiliated Traditional Chinese Medicine Hospital of Southwest Medical University, No. 182, Chunhui Road, Longmatan District, Luzhou, Sichuan, 646000, People's Republic of China, Tel +86 830 3160093, Fax +86 830 3160093, Email zhaoling-998@163.com

Purpose: The objective of this study was to develop long-circulating solid lipid nanoparticles (LSLN) containing a novel curcumin (CU) derivative (CU1), to improve CU1′s pharmacokinetic behavior and its anti-cancer effects in MHCC-97H liver cancer cells.

Methods: LSLN loaded with CU1 (CU1-LSLN) was optimized and characterized. The cell biological properties and the anti-cancer mechanism of CU1-LSLN on MHCC-97H cells were evaluated by MTT, flow cytometry, Transwell, and Western blot. CU1-LSLN was further evaluated for pharmacokinetic behavior, biodistribution, and liver toxicity in SD rats.

Results: The optimized CU1-LSLN formulation showed the ideal particle size (PS), polydispersity index (PDI), zeta potential (ZP), encapsulation efficiency (EE%), and drug loading (DL%) of 122.10 ± 6.63 nm, 0.19 ± 0.02, −36.30 ± 1.25 mV, 94.98 ± 0.90% and 4.53 ± 0.69%, respectively. X-ray powder diffraction (XRD), differential scanning calorimetry (DSC), and Fourier transform infrared spectrometry (FTIR) indicated that CU1 was well encapsulated by LSLN and existed in amorphous form. Storage stability of CU1-LSLN was up to 180 days with a sustained-release of drug over 96 h. The uptake efficiency of CU1-LSLN to MHCC-97H cells was 3.24 and 2.98 times higher than that of CU and CU1 after treatment for 3 h, which helped to enhance the inhibitive effect of CU1-LSLN on the proliferation, migration, and invasion potential of MHCC-97H cells and increased its ability to promote apoptosis. Meanwhile, the expression levels of NF-κB, COX-2, MMP-2, MMP-9, and uPA decreased significantly. In vivo, CU1-LSLN prolonged the retention time of the drug, the area under the curve (AUC) increased significantly (CU: 69.9-fold, CU1: 85.9-fold), and no significant liver toxicity was observed.

Conclusion: CU1-LSLN is a novel preparation with great potential for treating liver cancer.

Keywords: curcumin derivative, nanoparticle, MHCC-97H, pharmacokinetics

Received: 19 February 2022
Accepted: 1 May 2022
Published: 17 May 2022

Introduction

Hepatocellular carcinoma (HCC), the most common primary malignancy of the liver, is the second leading cause of cancer-related mortalities worldwide.[1,2] Dysregulation of apoptosis and high metastatic ability are the main reasons behind the low cure rate of HCC.[2,3] Therefore, inducing apoptosis and inhibiting migration and invasion are attractive treatment strategies for HCC. Chemotherapy is one of the primary methods for treating HCC and is especially important for patients who are unsuitable for or missed the opportunity of surgery.[4] However, the severe adverse effects of chemotherapy significantly affect patient compliance. Meanwhile, it has limited efficiency in controlling metastasis.[5] Therefore, it is imperative to identify and develop safe and effective chemotherapy drugs for HCC treatment.

An increasing number of natural active ingredients with anti-tumor bioactivities have been discovered in recent years. Among these, CU, extracted from the rhizome of the plant *Curcuma longa*, has a long history of use in traditional Chinese and Indian medicine.[6,7] Several pharmacological activities of CU have been revealed over the last few decades, such as anti-inflammatory,[8] anti-bacterial,[9] and particularly its anti-cancer activity, which is promising in the field of oncology.[10] However, relevant anti-cancer application of CU is hindered due to its physicochemical instability.[11]

To meet the needs for practical application against cancer, numerous derivatives of CU have been designed and investigated extensively.[12,13] In the previous study, our research group modified the structure of CU and synthesized the Curcumin derivative (CU1) by an esterification reaction.[14] The CU1 was shown to improve the stability of CU, increase its selectivity for liver cancer cells, decrease the cytotoxicity to normal liver cells (L02 cell line), and enhance the ability to induce apoptosis in HCC cells (SMMC-7721).[14] However, its pharmacokinetics and ability and mechanism of inhibiting HCC metastasis are still unclear.

The application of nanotechnology has made significant progress in the pharmaceutical field, with many new drugs introduced in the market during the past decade, such as Caplacizumab,[15] Abraxane,[16] and Vitoss.[17] For cancer therapy, nanomedicine shows distinctive advantages, including improved pharmacokinetics,[18] targeted release at the tumor site,[19] enhanced penetration and cellular uptake,[20] reversed multidrug resistance (MDR) of tumors,[21] and reduced toxicity[22] for chemotherapy drugs. Solid lipid nanoparticles (SLN) are among the cohort of promising drug delivery vehicles to appear in many anti-cancer drug development reports. In addition to the advantages of nano-formulations described above, several other features of SLN have been noted. The materials commonly used for SLN are natural or synthetic solid lipids with good biocompatibility.[23] Moreover, the freeze-dried SLN is kept in a solid-state at room temperature (RT), making it resistant to the effects of the external environment and improving drug stability.[24]

In this study, the CU1-LSLN drug delivery system was developed to improve the pharmacokinetics and the liver cancer metastasis inhibiting ability of CU1. The effects of CU1-LSLN on the proliferation, migration, invasion, and apoptosis of high metastatic liver cancer cells (MHCC-97H cells) were evaluated, and the mechanism was preliminarily explored. Pharmacokinetic experiments were conducted to investigate whether CU1-LSLN has sustained-release and long-circulation effects.

Materials and Methods

Chemicals

CU, methyl succinyl chloride, HSPC (Lipoid GmbH), and DSPE-PEG2000 (Lipoid GmbH) were purchased from the Luzhou Renkang Biotechnology Co., Ltd. CU1 was synthesized independently by professor Zhao Ling's team from Southwest Medical University. The structure and characteristics of CU1 are shown in Figure 1. All other chemicals were laboratory-grade reagents and used as such.

Cell Lines and Animals

MHCC-97H, a highly metastatic human HCC cell line, was a gift from the Department of Oncology, Affiliated Hospital of Southwest Medical University. The cell line was maintained as a continuous culture in high-glucose Dulbecco's modified Eagles medium (DMEM) (Gibco, Thermo Fisher Scientific, Inc.) with 10% fetal bovine serum (Hyclone, Utah, USA) in a humidified atmosphere with 5% CO_2 at 37°C. The Annexin V-FITC apoptosis detection kit was purchased from KeyGen Bio-Tech Co., Ltd., Nanjing, China.

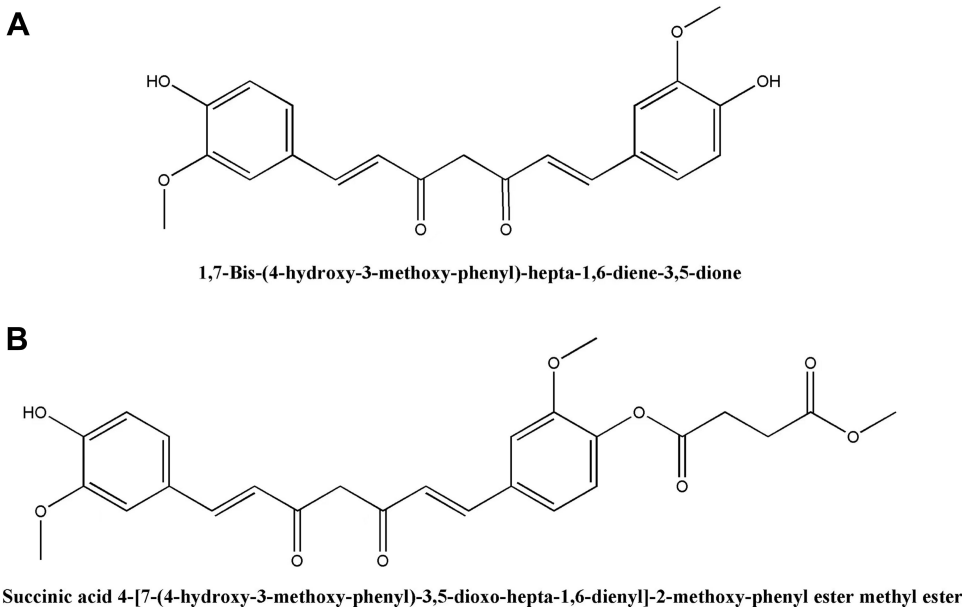

Figure 1 The structure of CU (**A**) and CU1 (**B**).

Male Sprague Dawley (SD) rats were purchased from the Chengdu Dashuo experimental animal Co., Ltd. (Sichuan, China, permit number: scxk (Chuan) 2018–181). The animals were housed in a climate- and light-controlled environment with free access to food and water. Rats used in the study weighed more than 200 g and had normal liver and kidney function. All the animals fasted overnight with free access to water before the experiment. Animal procedures were approved by the Committee on the Ethics of Animal Experiments of the Southwest Medical University for Nationalities, Luzhou, People's Republic of China (No 2015DW040). All the animal studies followed the Animal Welfare Act and were compliant with the regulations of Southwest Medical University and the National Institutes of Health Guide for the Care and Use of Laboratory Animals.

Preparation of CU1-LSLN

CU1-LSLN was prepared according to the improved thin-film ultrasonic dispersion method.[25] Briefly, the lipid phase comprising HSPC, DSPE-PEG2000, and CU1 was dissolved in 3 mL chloroform and evaporated at 150 rpm, in a rotary vacuum evaporator. This process was continued until a dry lipid film was deposited on the wall of the flask. Residual traces of solvent were removed using the vacuum dryer for 30 min at 37°C. Ultrapure water was used to hydrate the membrane. To obtain nano-sized particles, the dispersions were subjected to ultrasonic disruption (intensity 50%, 5 min). After sucrose (1.25%, w/v) was added as a freeze-dried protective agent, the LSLNs were frozen at −60°C and lyophilized by the freeze-drying system (LGJ-18C, Fourth-Ring Science Instrument plant Beijing Co., Ltd., Beijing, China) for 24 h to obtain a solid freeze-dried product.

Pharmaceutical Characterization

Determination of EE (%) and DL (%)

CU1 was a lipophilic substance, so during low-speed centrifugation, the free CU1 that was not encapsulated in LSLNs would form a precipitate. After the free drug was separated from the CU1-LSLN suspension (by centrifugation at 4000 rpm for 10 min), the supernatant dispersion (0.1 mL) was dissolved in a 6 mL mixture solution of methanol and ethyl acetate (4:1, v/v) and analyzed at 413 nm using the UV-visible spectrophotometer (Aoyi Instruments Shanghai Co., Ltd, Shanghai China) for the entrapped drug (W_e).[26] The total drug content (W_t) was determined using 0.1 mL of CU1-LSLN suspension without centrifugation.

Precisely weighed CU1-LSLN freeze-dried powder (W_0) was resuspended in ultrapure water. A mixture of methanol and ethyl acetate (4:1, v/v) was added to it to determine the total content of the drug (W_t).

The EE% and DL% were calculated according to the following formulas:

$$EE\% = W_e/W_t \times 100\%$$

$$DL\% = W_t/W_0 \times 100\%$$

Where W_t is the amount of total drug in CU1-LSLN suspension or freeze-dried powder, W_e is the amount of drug-loaded in LSLNs, and W_0 is the amount of total LSLN (including drug and other ingredients).

Measurement of PS, PDI, and ZP

The PS, PDI, and ZP of CU1-LSLN were measured by Malvern Zetasizer Nano series-ZS (Malvern Instruments, Malvern, Worcestershire, UK). Samples were diluted with ultrapure water to a fixed concentration and then analyzed in triplicates. Samples for ZP measurements are placed in special cuvettes with the capability to conduct current during the measurement. The electrophoretic mobility (μm/s) was converted to ZP by an in-built software using the Helmholtz-Smoluchowski equation.

XRD Analysis

XRD analysis of freeze-dried CU1-LSLN was performed using an X'D/MAX-2500/PC diffractometer (Rigaku Corporation, Tokyo, Japan) operating at 40 kV and 40 mA. Each sample was scanned between 0° and 90° in 2θ at the scanning rate of 8°/min.

DSC Analysis

DSC scans of the samples were performed with a microcalorimeter (TADSC25, USA) heated from 0°C to 200°C at a rate of 5°C/min under a nitrogen atmosphere.

FTIR Analysis

Using the Fourier transform infrared spectrometer (Shimadzu IRAffinity-1S, Japan), the spectra of each group of samples in the range of 4000–400 cm^{-1} were recorded.

Orthogonal Experimental Design

Based on the single factor, an orthogonal experimental design was applied to screen the optimal formulation of CU1-LSLN. Three factors of CU1-LSLN formulation, including the amount of CU1 (mg) (A), HSPC (mg) (B), and DSPE-PEG2000 (mg) (C), and three levels for each factor were selected and arranged according to an L_9 (3^3) orthogonal experimental table (Table 1). The comprehensive score (X) of EE% and DL% were used as the evaluation index. The comprehensive score (X) was calculated as follows.[14]

$$\text{Comprehensive score (X)} = Xn/Xmax \times 90 + Yn/Ymax \times 10$$

Xn and Yn are EE and DL under the n-th formulation, respectively. The Xmax and Ymax are the maximum values of EE and DL, respectively.

Table 1 The Factors and Levels of Orthogonal Design

Levels	Factors		
	A (CU1, mg)	B (HSPC, mg)	C (DSPE-PEG2000, mg)
1	7.0	35.0	14.0
2	6.0	30.0	12.0
3	5.0	25.0	10.0

Stability Estimation

The freeze-dried powder of CU1-LSLN was stored at RT and dispersed with ultrapure water to determine its PS, PDI, EE%, and DL% at various predetermined time points (0 d, 3 d, 5 d, 7 d, 14 d, 30 d, 90 d, and 180 d).

In vitro Release Study

To determine the release kinetics of CU1-LSLN, freeze-dried powder of CU1-LSLN was dispersed with ultrapure water. Later, 2 mL suspension (with 400 μg of CU1) was added into a dialysis bag (8 kDa molecular weight cutoff, Solarbio USA) and immersed into a 200 mL phosphate-buffered saline (PBS) buffer containing 10% (w/v) Tween-80. The stirred at a rate of 150 rpm and the temperature of 37 ± 0.5°C. Samples were withdrawn at predetermined time intervals. The same amount of fresh dissolution medium was added to maintain a constant volume. For comparison, a similar procedure of in vitro release study of free CU1 suspension was also conducted. Samples were analyzed by UV-visible spectrophotometer for drug content at 413 nm.

Three common models were used to fit the in vitro drug release kinetic models of each group of samples, and the fitting coefficient (r^2) was calculated.[27]

$$\text{Zero} - \text{order equations} : M_t = k_0 t + b$$

$$\text{First} - \text{order equations} : \ln(100 - M_t) = -k_1 t + b$$

$$\text{Higuchi equations} : M_t = k_h t^{1/2} + b$$

where M_t is the cumulative release at time t, the k_0, k_1, and k_h are the rate constants for the zero-order, first-order, and Higuchi equations, respectively.

Cellular Uptake Study by Flow Cytometry

Cellular uptake of CU1-LSLN by MHCC-97H cells was evaluated using fluorescent-active cell sorting (FACS, FACS Calibur flow cytometer with Cell Quest Software, BD Biosciences, Le Pont-de-Claix, France).[28] Briefly, 1×10^5 cells/well were seeded in 6-well plates and allowed to attach overnight at 37°C under a 5% CO_2 atmosphere. The cells were treated with a freshly prepared medium containing 20 μmol/L of CU, CU1, or an equivalent concentration of CU1-LSLN. Post-treatment, cells were incubated at 37°C under a CO_2 atmosphere for 1 or 3 h. Cells treated with the culture medium served as a negative control for the experiment. At the end of the incubation period, the cell monolayer was washed three times at RT with PBS to eliminate the excess drug and then trypsinized. The cells were collected by centrifugation at 1000 rpm for 4 min and dispersed in 1 mL PBS for analysis using FACS flow cytometer equipped with the 488 nm argon laser.

Cytotoxicity Study

The cytotoxicity of CU1-LSLN towards MHCC-97H cells, compared to CU and CU1, was evaluated by the MTT ([3-(4,5-dimethylthiazole-2-yl) −2,5-diphenyltetrazolium bromide]) assay.[13] Briefly, cells were seeded in 96-well plates at a density of 3×10^3 cells/well and cultured for 24 h. CU, CU1, and CU1-LSLN were then added to the wells with the final concentrations of 0, 6.25, 12.5, 25, 50, and 100 μg/mL and incubated for 24, 48, 72, and 96 h at 37°C. Dimethyl sulfoxide (DMSO, 0.1%) was used as a negative control. Then, 20 μL MTT solution (5 mg/mL) was added to each well and incubated for 3.5 h at 37°C. The medium was carefully removed, and 150 μL DMSO was added to each well to dissolve the formazan crystals and the absorbance was detected at 490 nm using the Multiskan Spectrum Microplate Reader (Thermo Fisher Scientific Inc.).

Apoptosis Assay

Annexin V/propidium iodide (PI) dual staining assay is a sensitive method implemented for the detection of apoptotic cells.[29] The protocol followed was according to the instruction manual. In brief, a total of 2×10^5 MHCC-97H cells were seeded into each well of 6-well plates and cultured for 24 h. Various concentrations (5, 10, and 20 μmol/L) of CU, CU1, and CU1-LSLN were added to the wells. The control group was treated with DMSO (0.1%) and medium, respectively.

Cells of each sample were harvested after an additional 24 h and suspended in 500 μL of Annexin V binding buffer (IX). Annexin V-FITC (5 μL) and 5μL of propidium iodide (PI) were added and incubated for 15 min in the dark. The cells were then analyzed by flow cytometry to identify and account for apoptotic cells.

Migration and Invasion Assay

Cell migration was analyzed with the aid of a Transwell chamber (Corning Incorporated, Corning, NY, USA) with 8-μm pores. Cell invasion assay was performed using a Corning Matrigel invasion chamber (Corning Incorporated). Cells suspended in 200 μL serum-free medium were seeded onto the upper chambers (1×10^5 cells/chamber for migration and 2×10^5 cells/chamber for invasion) and incubated with different concentrations of CU, CU1, and CU1-LSLN (5, 10, and 20 μmol/L). The chambers were placed into 24-well plates with a medium containing 10% serum. After 8 h, the cells remaining in the upper chamber were removed, and migrated or invaded cells on the lower membrane surface were fixed with 4% paraformaldehyde followed by staining with 0.1% crystal violet for 20 min. The randomly selected migrated or invaded cells in six visual fields (magnification, 200×) were counted in each transwell chamber under a phase-contrast microscope.

Western Blot Analysis

After treatment with 20 μmol/L CU, CU1, and CU1-LSLN, the cells were washed twice using ice-cold PBS (pH 7.4) and lysed in protein lysis buffer on ice. Total proteins were extracted by centrifuging the cell lysates at 10,000 rpm for 10 min at 4°C and the protein concentration was determined using the Bicinchoninic Acid (BCA) Protein Assay Kit (Beyotime Institute of Biotechnology, Shanghai, China). 50 μL protein from every sample was separated using 10% Sodium dodecyl-sulfate polyacrylamide gel electrophoresis (SDS-PAGE) gel and transferred to a polyvinylidene fluoride (PVDF) membrane. After blocking with Tris-buffered saline and Tween 20 (TBST) buffer containing 5% skimmed milk for 2 h at RT, the PVDF membrane was incubated with appropriate concentrations of primary antibodies (1:500 dilution) at 4°C overnight. After washing the membrane with TBST three times for 5 min, it was incubated with the corresponding secondary antibody (1:500 dilution) for 2 h at RT. Following three washes with TBST for 5 min, the immunoreactive bands were detected. β-actin was used as the internal control and the relative values of the target protein were corrected in accordance with the absorbency of the internal control.[2]

Pharmacokinetic Study

Animal Experiment

The rats were randomly assigned to three groups (n = 5). CU and CU1 were dissolved in a mixture of hydrogenated castor oil and ethanol (1:1, v/v). The formulations (CU1-LSLN suspension, CU, and CU1 solution) were administered by intravenous injection at a single dose of 15 mg/kg. Approximately 0.3 mL of blood was collected from the heart using a heparin-coated syringe at 2, 5, 10, 15, and 30 min, and at 1, 2, 4, 8, 12, 24, and 48 h after dosing. The blood was centrifuged at 3000 rpm for 10 min under refrigerated conditions, and the plasma was collected and stored at −70°C until high-performance liquid chromatography (HPLC) analysis.

Sample Extraction

A large number of preliminary experiments in the early stage found that CU1 and CU1-LSLN quickly converted to CU after entering the rat's body and mainly existed in the form of CU in the body. Therefore, the concentration of formulations in biological samples was analyzed as CU. CU was extracted from the plasma by a liquid-liquid extraction method. In brief, 50 μL of citric acid solution (0.05 g/mL) and acetonitrile 400 μL were added to the plasma in turn, and vortexed for 3 min. After centrifugation at 8000 rpm for 10 min, the supernatant was collected and evaporated to dryness at 45°C under nitrogen. The residue was reconstituted with 200 μL of mobile phase and centrifuged at 10,000 rpm for 10 min. The clear supernatant was injected into the HPLC system for analysis.

HPLC Analysis

Estimation of the drug content in plasma samples was conducted by reversed-phase HPLC (Agilent-1260, USA). The analysis was performed at 425 nm with an Inertsil ODS-SP C18, 5 μm, 4.6×250 mm column maintained at 25°C (made

in Japan). The mobile phase was composed of 35% water (containing 0.1% phosphoric acid, v/v) and 65% acetonitrile at a 1 mL/min flow rate.

Bio-Distribution in vivo

To observe the distribution of CU1-LSLN in vivo, fluorescent DiD dye and CU1 were co-encapsulated into LSLNs and injected intravenously into SD rats.[30,31] Fluorescence imaging of the heart, liver, lung, and kidney was performed at 1, 2, and 24 h after administration (excitation wavelength: 640 nm, emission wavelength: 730 nm).[30–32]

Liver Toxicity

Referring to the "Technical Guidelines for Acute Toxicity Testing of Chemical Drugs" issued by the Center for Drug Evaluation (CDE) of the State Drug Administration of China, SD rats were given a single high dose (50 mg/kg) of CU1-LSLN.[33] After 48 h of drug administration, liver tissues were taken, fixed with 10% phosphate-buffered formalin, embedded in paraffin, stained with H&E (hemAtoxylin-eosin), and observed under a light microscope.

Statistical Analysis

Pharmacokinetic parameters in plasma were calculated using a software program, DAS 2.0. All results were expressed as the mean ± standard deviation of at least three independent experiments and were analyzed using SPSS version 17.0 software (SPSS, Inc., Chicago, IL, USA). The statistical analysis was performed using the Student's *t*-test. $P < 0.05$ indicated a statistically significant difference.

Results

Optimized Formulation and Characterizations

The formulation of CU1-LSLN was optimized through an orthogonal design and the calculation was conducted using the software SPSS 17.0. The orthogonal result was shown in Table 2 and the variance analysis result was indicated in Table 3. Intuitively, the effects of each factor on the CU1-LSLN were as follows according to the range analysis: (B) the amount of HSPC > (A) CU1 > (C) DSPE-PEG2000. K1/3, K2/3, and K3/3 represented the mean value of each level. Analytical results of the three factors were: A: 2 > 1 > 3; B: 1 > 3 > 2; and C: 3 > 2 > 1. So the optimal parameters are A2B1C3. As shown in Table 3, through the variance analysis, factors A and B had a significant influence ($P < 0.05$) on the prepared CU1-LSLN. The result is consistent with range analysis. To sum up, the optimal formulation was as follows:

Table 2 The Design and Results of Orthogonal Table

No.	Levels			EE (%)	DL (%)	X
	A	B	C			
1	2	1	2	97.52	5.32	96.23
2	3	1	3	94.90	5.49	94.01
3	1	3	2	91.85	5.83	91.60
4	2	3	3	93.75	5.15	92.56
5	1	1	1	92.70	8.41	95.40
6	2	2	1	92.15	4.71	90.57
7	1	2	3	87.63	8.54	90.88
8	3	3	1	88.11	4.91	87.07
9	3	2	2	89.29	4.34	87.49
K1/3	92.60	95.21	91.01			
K2/3	93.12	89.65	91.77			
K3/3	89.52	90.41	92.48			
R	3.60	5.56	1.76			

Abbreviations: EE, encapsulation efficiency of CU1-LSLN; DL, drug loading of CU1-LSLN; X, comprehensive score; R, the range analysis.

Table 3 Variance Analysis Results

No.	Sum of Squares	Free Degree	Mean Square	F value	*P* value
A	22.81	2	11.41	33.40	0.03
B	54.64	2	27.32	80.02	0.01
C	3.24	2	1.62	4.75	0.17
Errors	0.68	2	0.34		

the amount of CU1, HSPC, and DSPE-PEG2000 was 6 mg, 35 mg, and 10 mg, respectively. And the PS of optimal CU1-LSLN formulation was 122.10 ± 6.63 nm with the PDI of 0.19 ± 0.02, and the ZP was 36.30 ± 1.25 -mV (Figure 2). Besides, EE and DL of CU1-LSLN were 94.98 ± 0.90% and 4.53 ± 0.69%, respectively.

Figure 3A showed the X-ray diffraction results of CU1, blank-LSLN, and CU1-LSLN. The crystalline CU1 had a series of diffraction peaks, but when CU1 was encapsulated in LSLN, the diffraction was similar to blank-LSLN. This indicated that CU1 might not exist in crystal form in LSLN.

The results of the DSC analysis were shown in Figure 3B. CU1 showed a sharp endothermic peak between 100–150 °C. However, this peak was not seen in CU1-LSLN, and the endothermic curves were similar to blank-LSLN. This thermal behavior suggested that CU1 was unable to crystallize. Therefore, CU1 existed in an amorphous form or molecularly dispersed in LSLN, which confirmed the results obtained by XRD.

FTIR (Figure 3C) showed that some of the characteristic peaks of CU1 were masked in CU1-LSLN, indicating that the crystal form of CU1 was well encapsulated by LSLN, which was consistent with the results of XRD and DSC.

Stability Study

The PS, PDI, and DL of CU1-LSLN were recorded at various time intervals during the 180 d study duration. As shown in Figure 4A, the changes in three indicators of CU1-LSLN were slight within 180 days, compared with the CU1-LSLN at the beginning of the experiment ($P > 0.05$). Moreover, on the 180th day, the coefficient of variation (CV, %) of PS,

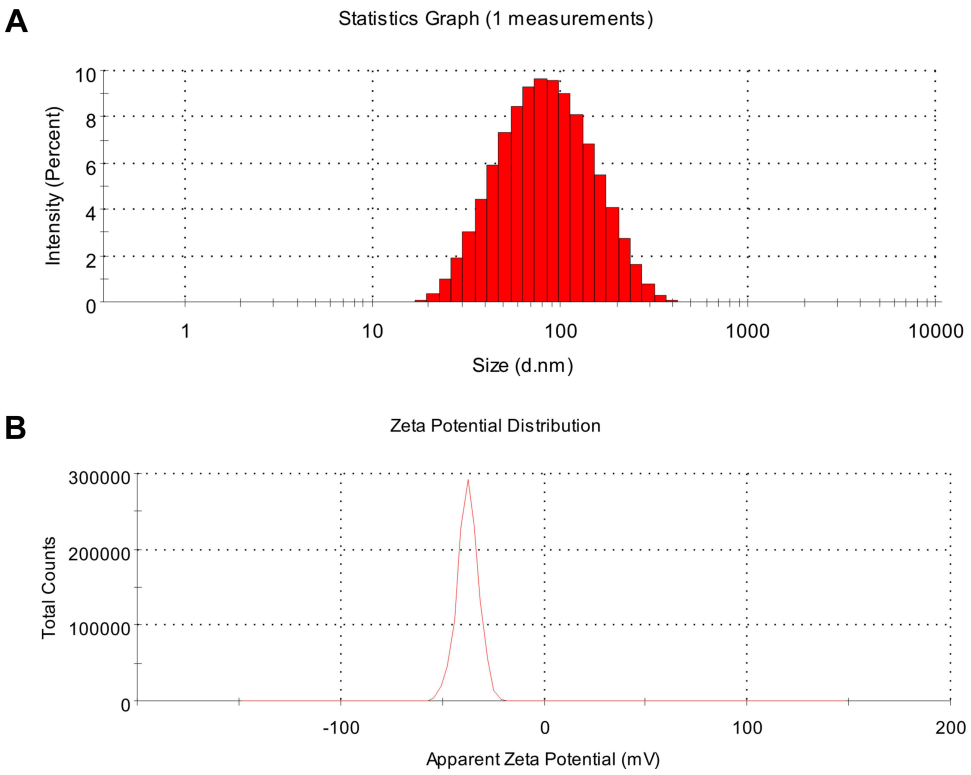

Figure 2 The particle size (**A**) and Zeta potential (**B**) of optimized CU1-LSLN.

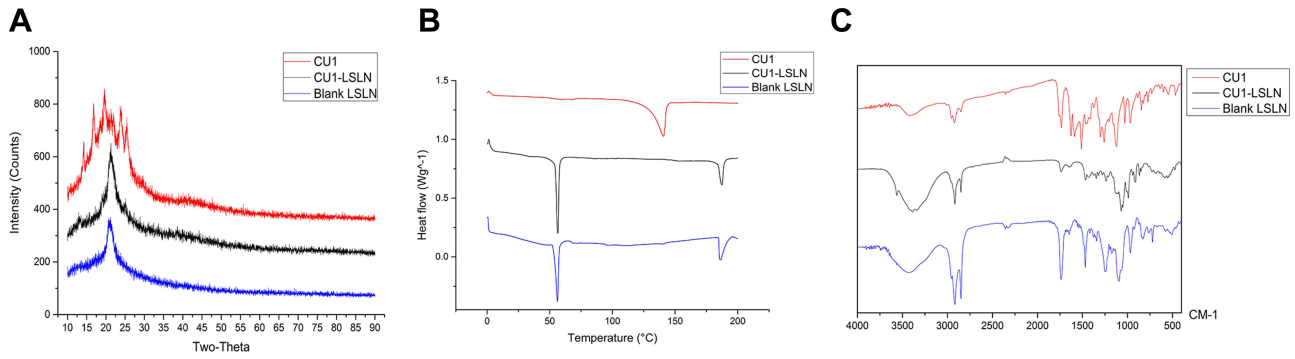

Figure 3 XRD (**A**), DSC (**B**), and FTIR (**C**) patterns.

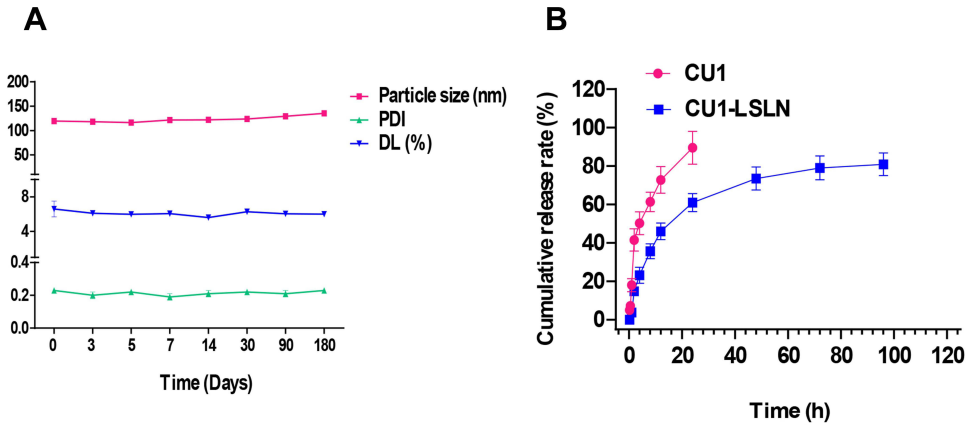

Figure 4 The results of stability test and in vitro release study. (**A**) The changes of particle size, PDI, DL of CU1-LSLN during the 180 days. (**B**) In vitro release profile of CU1 and CU1-LSLN.

PDI, and DL was 1.91%, 8.83%, and 6.73%, respectively, compared to 0 d, and the PDI was almost constant. The *P*-value was greater than 0.05, and there was no statistical difference. The results indicated that the CU1-LSLN freeze-dried samples maintained stability after storage at RT for 180 d.

In vitro Release Study

The release profiles of CU1 from CU1-LSLN and free CU1 suspension were displayed in Figure 4B. A cumulative percentage of 89.53% was released within 24 h for the free CU1 suspension compared to 60.98% for the CU1-LSLN. The cumulative release rate of free CU1 suspension remained unchanged after 24 h, while for CU1-LSLN, it increased from 60.98% to 80.93% at the end of 96 h. The fitting coefficients in different release models were shown in Table 4. For both CU1 and CU1-LSLN, the first-order equation provided the best fit. Nevertheless, the release constant k_1 was greatly reduced after being encapsulated by LSLN (CU1: 0.2374, CU1-LSLN: 0.0734). Therefore, the CU1-LSLN exhibited delayed drug release behavior over a 96-h period.

Table 4 Drug Release Kinetic Parameters and Fitting Coefficients

	Zero-Order Equation		First-Order Equation		Higuchi's Equation	
	r^2	k_0	r^2	k_1	r^2	k_h
CU1	0.7490	3.3640	0.9543	0.2374	0.9226	19.6434
CU1-LSLN	0.7355	0.8408	0.9922	0.0734	0.9180	9.3871

Abbreviations: r^2, fitting coefficient; K_0, K_1, and K_h are the rate constants for the zero-order, first-order, and Higuchi equations, respectively.

CU1-LSLN Enhanced the Uptake of CU1

Flow cytometry analysis (Figure 5A) revealed that the fluorescence intensity of CU1-LSLN was significantly higher than that of CU and CU1 solutions. Additionally, the fluorescence intensity of CU1-LSLN, CU, and CU1 at the end of 3 h was higher than that of 1 h. This uptake was depicted as a histogram (Figure 5B). Also, the mean fluorescence intensity in the cells was significantly increased by CU1-LSLN (3.16 and 2.93 times for 1 h; 3.24 and 2.98 times for 3 h) compared to CU and CU1 solutions. These results strongly indicated that the uptake of CU1-LSLN was significantly higher than CU and CU1 solutions, and the uptake efficiency was time-dependent.

CU1-LSLN Inhibited the Cell Proliferation in vitro

The anti-cancer profile of CU1-LSLN, compared to CU and CU1, was studied in the MHCC-97H cell line by calculating % inhibition. The results (Figure 6) showed that CU, CU1, and CU1-LSLN inhibited the proliferation of MHCC-97H cells in a dose- and time-dependent manner. The 96-hour inhibition rates of CU, CU1, and CU1-LSLN with maximum dose were 68.19 ± 1.19%, 71.83 ± 1.93%, and 94.32 ± 0.06%, respectively. The 48-hour inhibition rate of CU1-LSLN

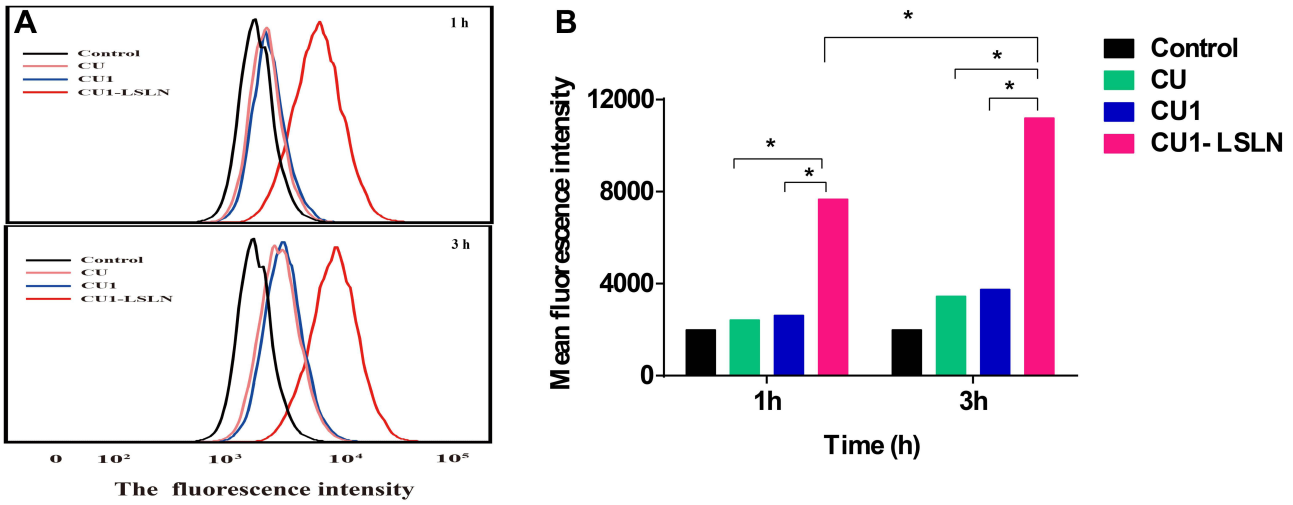

Figure 5 The uptake of CU1-LSLN by MHCC-97H cells. (**A**) Histogram showing uptake of CU, CU1 and CU1-LSLN by MHCC-97H cells using flow cytometry. (**B**) The mean fluorescence intensity of MHCC-97H cells after treatment with CU, CU1 and CU1-LSLN for 1 h and 3 h, respectively, *$P < 0.05$.

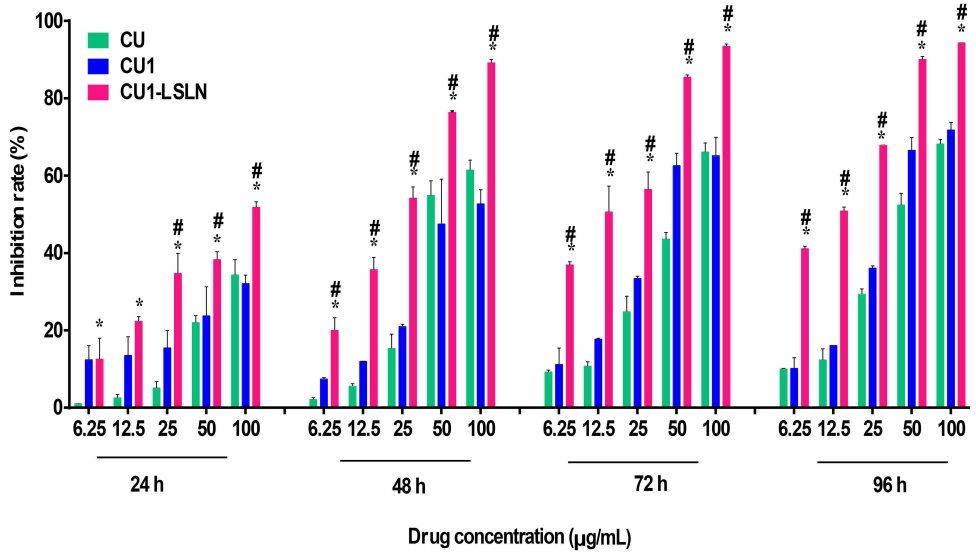

Figure 6 The effects of CU1-LSLN on MHCC-97H cells proliferation compared to CU and CU1. *$P < 0.05$ vs CU; #$P < 0.05$ vs CU1.

with maximum dose was 89.13 ± 0.88%, which was higher than the 96-hour inhibition rates of CU and CU1. Compared with CU and CU1, the inhibition rate of CU1-LSLN was significantly increased ($P < 0.05$). Based on the results above, CU1-LSLN exhibits enhanced anti-proliferation activity in MHCC-97H cells compared to CU and CU1.

CU1-LSLN Promoted Cell Apoptosis

The apoptosis-inducing effect of CU1-LSLN was analyzed using flow cytometry. After treatment with different concentrations of CU1-LSLN for 24 h with the CU and CU1 as controls, apoptosis induction was observed. As shown in Figure 7, the early apoptosis rate was higher than that of late apoptosis. The total apoptosis rates of MHCC-97H cells gradually increased as the concentration of drugs increased (Figure 7). The apoptosis rates of MHCC-97H cells induced by various concentrations of CU1-LSLN were 27.42 ± 0.23%, 41.23 ± 1.41%, and 44.16 ± 1.43%, respectively. These values were higher than that of CU (17.29 ± 0.66%, 25.74 ± 0.61%, and 33.11 ± 1.00%) and CU1 (29.56 ± 1.28%, 37.43 ± 1.56%, and 39.23 ± 0.49%) at the concentrations of 5, 10, and 20 μmol/L. These results suggested that CU1-LSLN exhibits a significantly higher apoptosis-inducing effect on MHCC-97H cells than CU and CU1, in a dose-dependent manner.

CU1-LSLN Inhibited Cell Migratory and Invasive Capacities

The transwell assay was performed to investigate CU1-LSLN's effects on the migration and invasion of MHCC-97H cells. The results were presented in Figure 8. The cell migration (%) of MHCC-97H cells treated with CU1-LSLN (5, 10, and 20 μmol/L) were 63.95 ± 3.32%, 44.68 ± 3.54%, and 23.26 ± 4.79%, respectively, which were significantly lower than that of cells treated with CU or CU1 ($P < 0.05$) (Figure 8A). Consistent with the cell migration results, the number of invasive cells in the CU1-LSLN group also decreased significantly compared to the CU and CU1 groups. The invasion capacity of MHCC-97H cells treated with CU1-LSLN (5, 10, and 20 μmol/L) decreased 9.31%, 29.52%, 34.57%, and 9.04%, 20.74%, 30.05%, respectively, compared to the cells treated with CU or CU1 (Figure 8B). Taken together, the above results indicated that CU1-LSLN enhances the suppression of cell migration and invasion in MHCC-97H cells compared to CU and CU1.

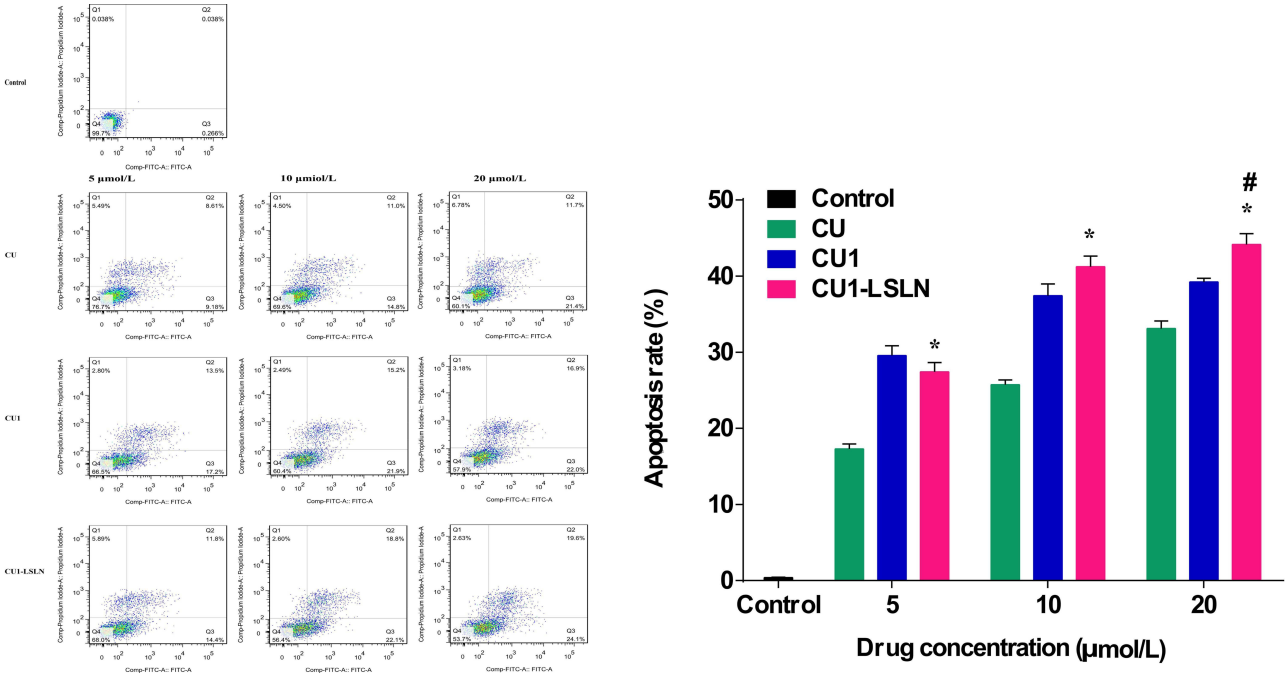

Figure 7 The effect of CU1-LSLN on apoptosis induction. The MHCC-97H cells (2×10^5 cells/well) were treated with CU, CU1 and CU1-LSLN (5, 10, 20 μmol/L) then were analyzed by Annexin V-PI staining flow cytometry. *$P < 0.05$ vs CU; #$P < 0.05$ vs.CU1.

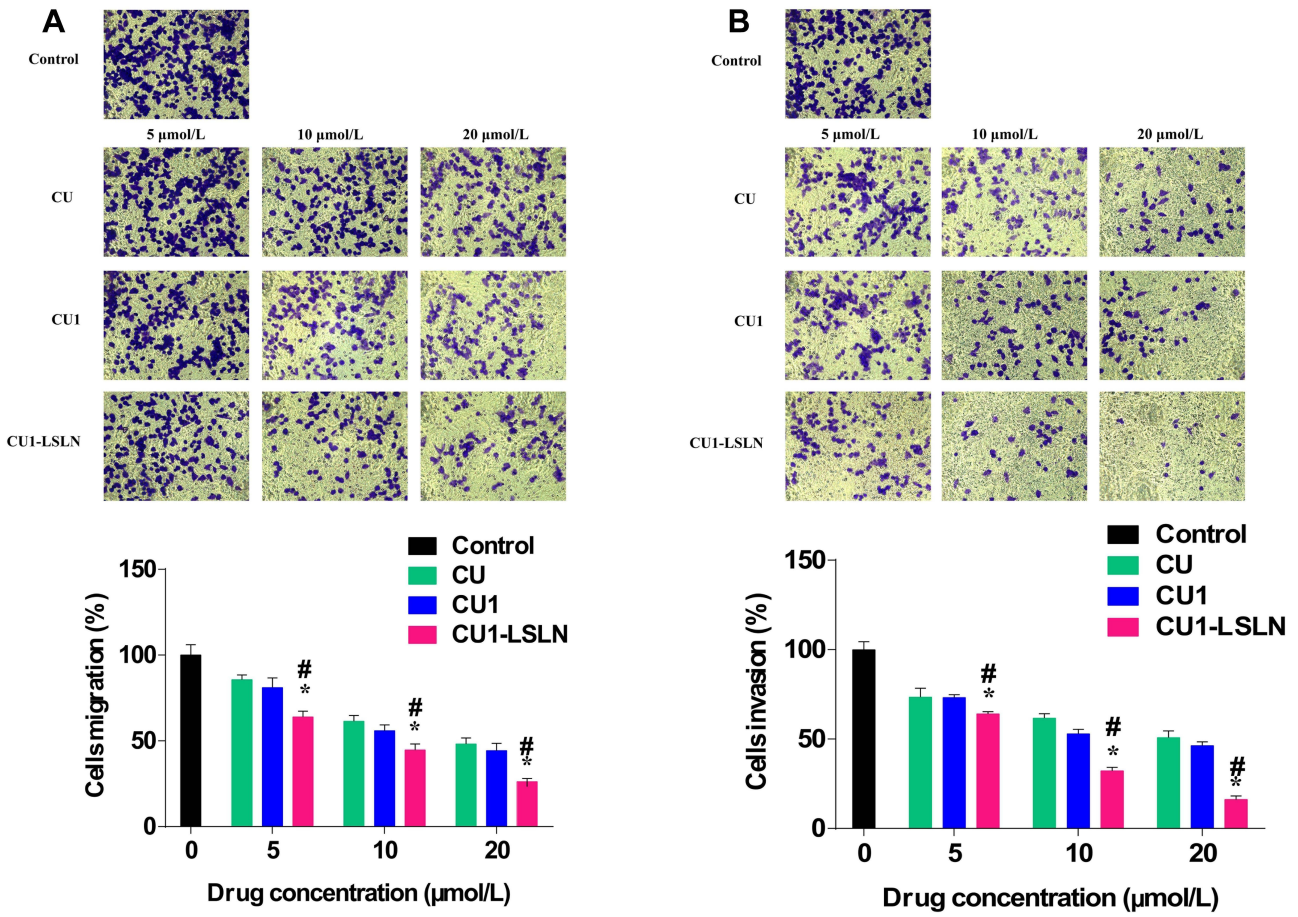

Figure 8 The effect of CU1-LSLN on cell migration and invasion in MHCC-97H cells compared to CU and CU1. (**A**) Representative images of migration cells stained with crystal violet. Columns, the mean migration rate (%) from three different experiments with three duplicates. (**B**) Representative images of invasive cells stained with crystal violet. Columns, the mean invasion rate (%) from three different experiments with three duplicates. $^{*}P < 0.05$ vs CU; $^{\#}P < 0.05$ vs.CU1.

CU1-LSLN Decreased the Expression of Anti-Metastatic Proteins and NF-κB Activation

MHCC-97H cells were treated with 20 μmol/L CU1-LSLN (the same concentrations of CU and CU1 as controls) for 24 h. Figure 9 showed a Western blotting analysis of the protein levels of MMP-2, MMP-9, COX-2, and uPA. Protein levels of MMP-2, MMP-9, COX-2, and uPA of the CU1-LSLN group decreased significantly compared to the CU group ($P < 0.05$).

In addition to these proteins, we found that CU1-LSLN can also inhibit the activation of the NF-κB signal pathway, and this inhibitory effect of CU1-LSLN was significantly higher than that of CU ($P < 0.05$) and slightly higher than that of CU1 (Figure 9).

CU1-LSLN Improved the Pharmacokinetic Behavior

DAS 2.1.1 software was used to process the concentration-time data of each group of CU to obtain the main kinetic parameters of each group, as shown in Table 5. The results showed that there was no obvious advantage after CU was modified to CU1. Interestingly, after preparing CU1 into LSLN, the AUC of the CU1-LSLN group was significantly increased (CU: 69.9-fold, CU1: 85.9-fold), the Mean Residence Time (MRT) (0-t), and the Maximum Concentration (C_{max}) were 4.4 and 4.6 times higher than CU and 12.8 and 2 times than CU1, respectively. And the clearance rate (CL_z) of CU1-LSLN was significantly reduced. After 24 h of administration, no drug was detected in the plasma of the CU and CU1 groups. Contrastingly, high blood drug concentration was detected at 48 h in the CU1-LSLN group, indicating that loading the drug with nanoparticles can prolong the action time of the drug in the body. Therefore, it can be concluded

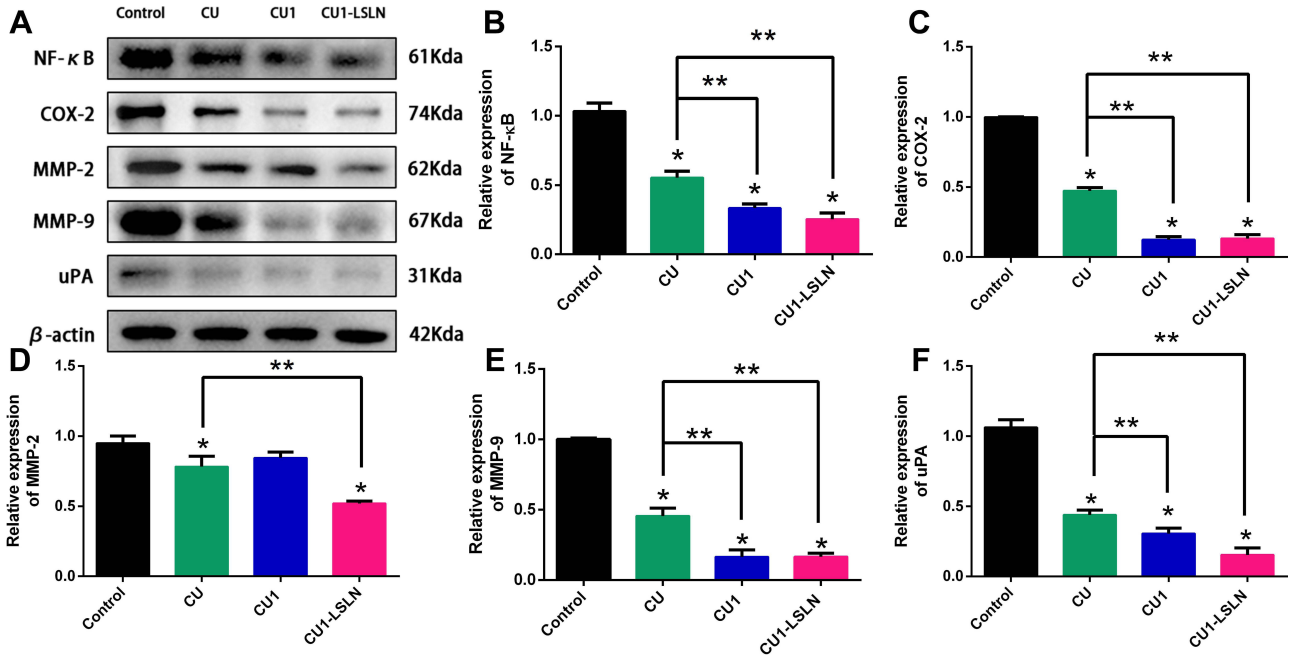

Figure 9 Expression of cells by Western blot (**A**), and quantitative analysis (**B**–**F**). * vs control $P < 0.05$; ** vs CU $P < 0.05$.

that at the same dose, CU1-LSLN can increase the blood concentration to a certain extent and prolong the action time of the drug in the body, which may produce better anti-cancer effects.

Bio-Distribution of CU1-LSLN in vivo

Figure 10A shows the distribution of CU1-LSLN in rats. Significant fluorescence can be observed in the liver, with a much higher intensity than in other tissues. Moreover, comparing the results at 1 and 2 h, the fluorescence intensity in every tissue increases significantly over time, especially in the liver. After 24 h of administration, the fluorescence intensity in the liver decreased. Still, the fluorescence intensity in the lung and heart increased slightly, and the fluorescence intensity in the kidney remained unchanged.

Toxicity of CU1-LSLN in Liver

H&E staining showed that the liver tissue had a complete capsule, the hepatic lobules were indistinct, the central vein endothelial cells were relatively intact, the hepatocytes were arranged radially around the central vein, and the morphology of the hepatocytes was normal (Figure 10B). No apparent pathological changes were seen.

Table 5 The Main Pharmacokinetic Parameters After Given CU, CU1, or CU1-LSLN by Tail Vein Injection

Parameter	Unit	CU	CU1	CU1-LSLN
$AUC_{(0-t)}$	mg/L*min	2.51	2.04	175.43
$MRT_{(0-t)}$	min	142.89	49.14	632.31
$t_{1/2z}$	min	160.86	40.62	1642.76
T_{max}	min	10	10	15
V_z	L/kg	1268.93	426.65	96.57
CL_z	L/min/kg	5.47	7.28	0.041
C_{max}	mg/L	0.043	0.10	0.20

Abbreviations: AUC, area under the curve; MRT, mean residence time; $t_{1/2z}$, half-life; T_{max}, time of maximum concentration; V_z, apparent volume of distribution; CL_z, clearance rate; C_{max}, maximum concentration.

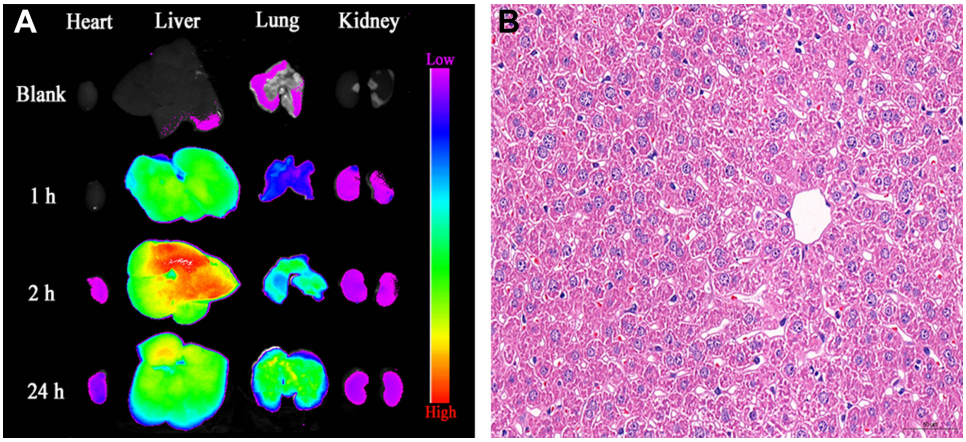

Figure 10 (**A**) Fluorescence images of organs at 1 h, 2 h, and 24 h after CU1-LSLN was injected into tail vein. (**B**) H&E staining of liver.

Discussion

In a previous study, we synthesized and purified CU1. Briefly, using triethylamine as a catalyst, CU was reacted with methyl succinyl chloride in dichloromethane. The crude product was purified by silica gel column chromatography to obtain the corresponding CU1 solution and concentrated and dried to obtain a yellow solid (ESI-MS m/z 483.16 [M+H]+, the melting point is 140–145°C).[14] The CU1 modified by our group had similar anti-proliferative activity in HCC as CU but with improved stability. However, the pharmacological properties of CU1 are still unclear. At a deeper level, its anti-proliferative and anti-metastasis effects in HCC and its mechanism need further research. SLN has the advantages of improving the bio-distribution of existing anticancer drugs and prolonging accumulation in the bloodstream and tumor.[34] In the current study, a solid lipid nano-level delivery system (CU1-LSLN) was successfully developed using HSPC and DSPE-PEG2000 via a simple thin-film hydration method to enhance the anti-cancer activity of CU1 and prolong its retention time in vivo.

The optimized CU1-LSLN showed a small PS and a normal distribution with a relatively low PDI (< 0.3), which could affect the uptake by the reticuloendothelial system, and thereby increase the absorption alongside bioavailability of the drug, leading to passive accumulation in tissues.[35] The ZP value is used to evaluate the physical stability of nano-formulations during storage.[36] Due to the electrostatic repulsion between adjacent particles, the particles keep a certain distance, thus reducing the aggregation and contributing to the stability of the nanosuspension. Generally speaking, the negative charge on the surface can prevent particles from combining with plasma protein, thus improving the stability of the particles in the blood and prolonging their circulation.[37] In this study, the ZP value of CU1-LSLN was −36.30 ± 1.25 mV, indicating that this system was stable In terms of stability, the CU1-LSLN freeze-dried samples were stable within six months, and it remains to be determined whether the samples can be stored for a longer time at RT. Besides PS, PDI, and ZP, the choice of lipid membrane material is also a significant factor affecting the stability of the particles. As we all know, when phospholipids undergo a phase transition, phase separation occurs, increasing the membrane's fluidity and leakage of the contents. Therefore, LSLN with higher phase transition temperatures (T_m) has higher membrane stability and lower drug release rates.[38] All phospholipids have a specific T_m value. Generally, the longer the acyl side chain, the higher the T_m. To improve the stability of the membrane and prevent the leakage of drugs, HSPC with a longer aliphatic chain and higher T_m was selected as the main excipient in this study. Some studies have shown that DSPE-PEG2000 can also assist HSPC in forming more stable particles.[39] However, different proportions of formula will affect the lipid membrane composition and strongly influence the performance of the SLN. Therefore, through the orthogonal design, the best ratio of HSPC, DSPE-PEG2000, and CU1 was screened, which led to the satisfactory performance of CU1-LSLN in vitro.

In an in vitro release study, the free CU1 group displayed an almost complete release within 24 h, while the CU1 from LSLN was sustained and continued till 96 h. The release pattern could be divided into two stages. At the first stage, the CU1-LSLN had a rapid release, which might be due to a certain CU1 being adsorbed onto the surface of LSLN, whereas the sustained release profile at the late stage suggests the diffusion of CU1 from the core of the lipid matrix to the release

medium.[40,41] These results proved that CU1 could be released slowly from CU1-LSLN and maintain a constant concentration for a comparatively longer period than the free CU1 suspension.

HCC is one of the most common malignant tumors globally. Invasion and metastasis are essential biological characteristics, and the root causes of deaths in HCC patients.[42] Previous research revealed that CU, a traditional medicine in Asia, could promote apoptosis and inhibit tumorigenesis in vitro.[43,44] Its anti-cancer activities are mainly due to the inhibition of proliferation, migration, and invasion, as well as on account of the induction of apoptosis.[45,46] In the present study, the newly developed CU1-LSLN showed better advantages in inhibiting the proliferation, migration, and invasion of MHCC-97H cells and inducing apoptosis compared with CU and CU1. The enhancement of the inhibition and induction observed in CU1-LSLN may be due to the enhanced cellular uptake of the drug by LSLN.[29] The transport of drug-loaded particles into cells is the key to its function, and the specific internalization methods mainly include endocytosis or fusion. However, lipid membranes with good biocompatibility are more likely to fuse with cell membranes and thus exhibit higher cellular uptake properties. Generally speaking, the materials commonly used in LSLN are natural or synthetic solid lipids, which have good biocompatibility. And the results of this study also support this claim that LSLN can enhance the cellular uptake of drugs.

In general, metastasis of cancer cells involves multiple processes and various cytophysiological changes. The degradation or breakdown of the extracellular matrix (ECM) through protease is a critical step in tumor invasion or migration. MMP-2, MMP-9, and uPA reportedly play crucial roles in cancer invasion and metastasis. They can degrade and decompose ECM, prompting cancer cells metastasis.[47] COX-2, an inducible immediate response gene, is closely related to lymph node metastasis, differentiation, and depth of invasion of various tumors such as colon and lung cancer.[48,49] NF-κB is a crucial regulator for the transcriptional inhibition of MMPs and uPA.[4] In this study, we verified that the suppressive effect of CU1-LSLN on MHCC-97H cell proliferation, migration, and invasion might be via inhibiting the activation of the NF-κB signaling pathway and down-regulating the protein expression of MMP-2, MMP-9, COX-2, and uPA. A similar finding was reported by Zhu et al that CU suppressed the proliferation, migration, and invasion in human lung adenocarcinoma LTEP-A2 cells by down-regulation of COX-2 and MMP-9 expression.[49] Besides, this study's data also indicated that the protein levels of NF-κB, MMP-2, MMP-9, and uPA in the CU1-LSLN group were lower than those in the CU and CU1 group, which may be due to the higher uptake efficiency of CU1-LSLN. However, some studies have also reported that CU could inhibit the migration and invasion of non-small cell lung cancer cells through the suppression of PI3K/AKT/mTOR signaling pathway.[50] Thus, CU1-LSLN may use different pathways or protease to achieve the anti-metastasis effect in HCC. Further studies are required to substantiate any other anti-metastasis mechanisms and protease expression of CU1 and CU1-LSLN.

The results of pharmacokinetic studies serve as an important indicator for evaluating drug metabolic behavior. The experiment results suggested that CU1-LSLN exhibits significantly increased relative bioavailability and improved pharmacokinetic behavior, which may be due to the unique metabolic behavior of LSLN itself. HSPC as an amphoteric surfactant, its hydrophobic core should be able to carry highly insoluble drugs with high loading capacity, while its hydrophilic moiety provides steric protection and improves the water solubility of insoluble drugs.[34,51] PEGylated nanoparticles have great potential in shielding the nanoparticles from reticuloendothelial system (RES). This is due to steric repulsion resulting from a loss of configurational entropy of the bound PEG chains and their rapid motion in aqueous media. Furthermore, hydrophilic PEG can form a hydrated surface, thereby protecting the nanoparticles from being quickly taken by the RES, thus extending the half-life of drugs and their tissue distribution.[52,53] In addition, CU1-LSLN was primarily distributed in the liver and was safe for the liver, suggesting the feasibility of its use in therapies for liver diseases, including liver cancer.

Conclusion

CU1-LSLN displayed a small PS with uniform distribution, high encapsulation rate, sustained-release behavior in vitro, and desired stability. CU1-LSLN could enhance the uptake efficiency, resulting in improved inhibition of proliferation, invasion, migration, and increased apoptosis induction in MHCC-97H cells compared to free CU or CU1. The anti-migration and anti-invasion effects of CU1-LSLN on MHCC-97H cells appear to be via inhibition of the activation of the NF-κB signaling pathway, and thereby down-regulation of the protein expression levels of MMP-2, MMP-9, COX-2 and

uPA. In vivo, CU1-LSLN increased the AUC and prolonged the duration of the drug's effect on the body. Therefore, CU1-LSLN is a promising agent for the treatment of liver cancer.

Acknowledgments

This study was supported by the Cooperative Scientific Research Project of Chunhui Plan of the Ministry of Education of China (No. 2020-703), the Youth Science and Technology Innovation Research Team (No. 2021JDTD0008), and the Basic Research Fund (No. 2020YJ0336, 2020YJ0373) of the Science and Technology Department of Sichuan province of China, Science and Technology Innovation Team from Jiucheng Science and Technology Talent Cultivation Plan in Luzhou City (No. 2019-1). Key Research and Development Projectors of Office of Science & Technology and Talent Work of Luzhou (No. 2021-SYF-26).

Disclosure

The authors report no conflicts of interest in this work.

References

1. Cortes J, Perez-García JM, Llombart-Cussac A, et al. Enhancing Global Access to Cancer Medicines. *CA Cancer J Clin*. 2020;70:105–124.
2. Chen WT, Hsu FT, Liu YC, et al. Fluoxetine Induces Apoptosis through Extrinsic/Intrinsic Pathways and Inhibits ERK/NF-κB-Modulated Anti-Apoptotic and Invasive Potential in Hepatocellular Carcinoma Cells In Vitro. *Int J Mol Sci*. 2019;20:757–772.
3. Fabregat I. Dysregulation of apoptosis in hepatocellular carcinoma cells. *World J Gastroenterol*. 2009;15:513–520.
4. Guo P, Pi C, Zhao S, et al. Oral co-delivery nanoemulsion of 5-fluorouracil and curcumin for synergistic effects against liver cancer. *Expert Opin Drug Deliv*. 2020;17:1473–1484.
5. Chen TW, Yin FF, Yuan YM, et al. Promotes Liver Cancer Metastasis by Facilitating Rab14 Recycle. *Nat Commun*. 2019;10(1):10–25.
6. Vecchione R, Quagliariello V, Calabria D, et al. Curcumin bioavailability from oil in water nano-emulsions: in vitro and in vivo study on the dimensional, compositional and interactional dependence. *J Control Release*. 2016;233:88–100.
7. Kunnumakkara AB, Harsha C, Banik K, et al. Is Curcumin Bioavailability a Problem in Humans: lessons From Clinical Trials. *Expert Opin Drug Metab Toxicol*. 2019;15(9):705–733.
8. Ułamek-Kozioł M, Czuczwar SJ, Januszewski S, et al. Substantiation for the Use of Curcumin During the Development of Neurodegeneration After Brain Ischemia. *Int J Mol Sci*. 2020;21(2):517.
9. Sadeghianmaryan A, Yazdanpanah Z, Soltani YA, et al. Curcumin-loaded Electrospun Polycaprolactone/Montmorillonite Nanocomposite: wound Dressing Application With Anti-Bacterial and Low Cell Toxicity Properties. *J Biomater Sci Polym Ed*. 2020;31(2):169–187.
10. Rodrigues FC, Anil Kumar NV, Thakur G. Developments in the anticancer activity of structurally modified curcumin: an up-to-date review. *Eur J Med Chem*. 2019;177:76–104.
11. Santezi C, Reina BD, Dovigo LN. Curcumin-mediated Photodynamic Therapy for the Treatment of Oral infections-A Review. *Photodiagnosis Photodyn Ther*. 2018;21:409–415.
12. Mhd AT, Roja H, Zhao X. A Review of Curcumin and Its Derivatives as Anticancer Agents. *Int J Mol Sci*. 2019;20(5):1–26.
13. Mu J, Wang X, Dong L, et al. Curcumin Derivative L6H4 Inhibits Proliferation and Invasion of Gastric Cancer Cell Line BGC-823. *J Cell Biochem*. 2019;120(1):11–17.
14. Feng T. Preparation of naturally effective monomer CU derivative (CU1), construction and evaluation of its nanoparticle delivery system (CU1-SLN). *Southwest Medical University*. 2018;3:42.
15. Sean D. Caplacizumab: first Global Approval. *Drugs*. 2018;78(15):39–42.
16. Gianni L, Mansutti M, Anton A, et al. Comparing Neoadjuvant Nab-paclitaxel vs Paclitaxel Both Followed by Anthracycline Regimens in Women With ERBB2/HER2-Negative Breast Cancer-The Evaluating Treatment With Neoadjuvant Abraxane (ETNA) Trial: a Randomized Phase 3 Clinical Trial. *JAMA Oncol*. 2018;4(3):302–308.
17. Westhauser F, Essers C, Karadjian M, et al. Supplementation With 45S5 Bioactive Glass Reduces In Vivo Resorption of the β-Tricalcium-Phosphate-Based Bone Substitute Material Vitoss. *Int J Mol Sci*. 2019;20(17):1–10.
18. Pathade AD, Kommineni N, Bulbake U, et al. Preparation and Comparison of Oral Bioavailability for Different Nano-formulations of Olaparib. *AAPS PharmSciTech*. 2019;20(7):276–289.
19. Truffi M, Mazzucchelli S, Bonizzi A, et al. Nano-Strategies to Target Breast Cancer-Associated Fibroblasts: rearranging the Tumor Microenvironment to Achieve Antitumor Efficacy. *Int J Mol Sci*. 2019;20(6):1–18.
20. Liu X, Jiang J, Meng H. Transcytosis - An Effective Targeting Strategy That Is Complementary to "EPR Effect" for Pancreatic Cancer Nano Drug Delivery. *Theranostics*. 2019;9(26):18–25.
21. Lim C, Moon J, Sim T, et al. A Nano-Complex System to Overcome Antagonistic Photo-Chemo Combination Cancer Therapy. *J Control Release*. 2019;295:164–173.
22. Chugh H, Sood D, Chandra I, et al. Role of Gold and Silver Nanoparticles in Cancer Nano-Medicine. *Artif Cells Nanomed Biotechnol*. 2018;46:10–20.
23. Chetoni P, Burgalassi S, Monti D, et al. Solid lipid nanoparticles as promising tool for intraocular tobramycin delivery: pharmacokinetic studies on rabbits. *Eur J Pharm Biopharm*. 2016;109:214–223.
24. Doktorovova S, Shegokar R, Souto EB. Role of excipients in formulation development and biocompatibility of lipid nanoparticles (SLN/NLCs). *Nanostructures for Novel Therapy*. 2017;1:811–843.

25. Parhi P, Suklabaidya S, Kumar Sahoo S. Enhanced Anti-Metastatic and Anti-Tumorigenic Efficacy of Berbamine Loaded Lipid Nanoparticles in Vivo. *Sci Rep*. 2017;7(1):5806–5819.
26. Umang S, Garima J, Krutika S. Improvement in Antihypertensive and Antianginal Effects of Felodipine by Enhanced Absorption From PLGA Nanoparticles Optimized by Factorial Design. *Mater Sci Eng C Mater Biol Appl*. 2014;35:153–163.
27. Wei YM, Xue ZK, Wang P, et al. Formulation and pharmacokinetic evaluation of once-daily sustained-released system of nifedipine with solid dispersion and coating techniques. *Arch Pharm Res*. 2013;36(7):864–873.
28. Thiramanas R, Jiang S, Simon J, et al. Silica Nanocapsules with Different Sizes and Physicochemical Properties as Suitable Nanocarriers for Uptake in T-Cells. *Int J Nanomedicine*. 2020;15:6069–6084.
29. Pindiprolu SKSS, Chintamaneni PK, Krishnamurthy PT, et al. Formulation-optimization of solid lipid nanocarrier system of STAT3 inhibitor to improve its activity in triple negative breast cancer cells. *Drug Dev Ind Pharm*. 2019;45(2):304–313.
30. Luo H, Lu L, Liu N, et al. Curcumin loaded sub-30 nm targeting therapeutic lipid nanoparticles for synergistically blocking nasopharyngeal cancer growth and metastasis. *J Nanobiotechnology*. 2021;19:224.
31. Tan L, Peng J, Zhao Q, et al. A Novel MPEG-PDLLA-PLL Copolymer for Docetaxel Delivery in Breast Cancer Therapy. *Theranostics*. 2017;7:2652–2672.
32. Deng C, Zhang Q, He P, et al. Targeted apoptosis of macrophages and osteoclasts in arthritic joints is effective against advanced inflammatory arthritis. *Nat Commun*. 2021;12:2174.
33. Xiao L, Bei Y, Li J, et al. Preclinical Pharmacokinetics, Tissue Distribution and Primary Safety Evaluation of a Novel Curcumin Analogue H10 Suspension, a Potential 17β Hydroxysteroid Dehydrogenase Type 3 Inhibitor. *Chem Pharm Bull (Tokyo)*. 2021;69(1):52–58.
34. Parveen S, Sahoo SK. Long circulating chitosan/PEG blended PLGA nanoparticle for tumor drug delivery. *Eur J Pharmacol*. 2011;670:372–383.
35. Wei Q, Yang Q, Wang Q, et al. Formulation, Characterization, and Pharmacokinetic Studies of 6-Gingerol-Loaded Nanostructured Lipid Carriers. *AAPS PharmSciTech*. 2018;19(8):3661–3669.
36. Jia L, Shen J, Zhang D, et al. In vitro and in vivo evaluation of oridonin-loaded long circulating nanostructured lipid carriers. *Int J Biol Macromol*. 2012;50:523–529.
37. Feng X, Pi C, Fu S, et al. Combination of curcumin and paclitaxel liposomes exhibits enhanced cytotoxicity towards A549/A549-T cells and unaltered pharmacokinetics. *J Biomed Nanotechnol*. 2020;16:1304–1313.
38. Chen J, Cheng D, Li J, et al. Influence of lipid composition on the phase transition temperature of liposomes composed of both DPPC and HSPC. *Drug Dev Ind Pharm*. 2013;39(2):197–204.
39. Zhang J, Liang H, Yao H, et al. The preparation, characterization of Lupeol PEGylated liposome and its functional evaluation in vitro as well as pharmacokinetics in rats. *Drug Dev Ind Pharm*. 2019;45(7):1052–1060.
40. Omwoyo WN, Melariri P, Gathirwa JW, et al. Development, characterization and antimalarial efficacy of dihydroartemisinin loaded solid lipid nanoparticles. *Nanomedicine*. 2016;12(3):801–809.
41. Tian L, Gao J, Yang Z, et al. Tamibarotene-Loaded PLGA Microspheres for Intratumoral Injection Administration: preparation and Evaluation. *AAPS PharmSciTech*. 2018;19(1):275–283.
42. Yeh CB, Hsieh MJ, Hsieh YH, et al. Antimetastatic Effects of Norcantharidin on Hepatocellular Carcinoma by Transcriptional Inhibition of MMP-9 through Modulation of NF-kB Activity. *PLoS One*. 2012;7(2):e31055.
43. Ardito F, Perrone D, Giuliani M, et al. Ardito, Effects of curcumin on squamous cell carcinoma of tongue: an in vitro study. *Curr Top Med Chem*. 2018;18(3):233–243.
44. Li Y, Sun W, Han N, et al. Curcumin inhibits proliferation, migration, invasion and promotes apoptosis of retinoblastoma cell lines through modulation of miR-99a and JAK/STAT pathway. *BMC Cancer*. 2018;18:1230–1239.
45. Alakhova DY, Kabanov AV. Pluronics and MDR reversal: an update. *Mol Pharm*. 2014;11(8):2566–2578.
46. Weng CJ, Chau CF, Hsieh YS, et al. Lucidenic acid inhibits PMA-induced invasion of human hepatoma cells through inactivating MAPK/ ERK signal transduction pathway and reducing binding activities of NF-kappaB and AP-1. *Carcinogenesis*. 2008;29:147–156.
47. Gialeli C, Theocharis AD, Karamanos NK. Roles of matrix metalloproteinases in cancer progression and their pharmacological targeting. *FEBS J*. 2011;278:16–27.
48. Liu JF, Zhang SW, Jamieson GG, et al. The effects of a COX-2 inhibitor meloxicam on squamous cell carcinoma of the esophagus in vivo. *Int J Cancer*. 2008;122(7):1639–1644.
49. Mingao Z, Lei C. Inhibition of curcumin on human lung adenocarcinoma LTEP-A2 cells and its mechanism. *Pak J Pharm Sci*. 2019;32:1307–1311.
50. Wang N, Feng T, Liu X, et al. Curcumin inhibits migration and invasion of non-small cell lung cancer cells through up-regulation of miR-206 and suppression of PI3K/AKT/mTOR signaling pathway. *Acta Pharm*. 2020;70(3):399–409.
51. Erel-Akbaba G, Carvalho LA, Tian T, et al. Radiation-Induced Targeted Nanoparticle-Based Gene Delivery for Brain Tumor Therapy. *ACS Nano*. 2019;13(4):4028–4040.
52. Otsuka H, Nagasaki Y, Kataoka K. PEGylated nanoparticles for biological and pharmaceutical applications. *Drug Delivery Rev*. 2003;55:403–419.
53. Vonarbourg A, Passirani C, Saulnier P, et al. Parameters influencing the stealthiness of colloidal drug delivery systems. *Biomaterials*. 2006;27:4356–4373.